Acta Biomaterialia 6 (2010) 2580–2589

Contents lists available at ScienceDirect

Acta Biomaterialia

journal homepage: www.elsevier.com/locate/actabiomat

Microtopographically patterned surfaces promote the alignment of tenocytes and extracellular collagen

Ashish Kapoor [a,c,1], Evelyn H.G. Caporali [b,c,1], Paul J.A. Kenis [a,c], Matthew C. Stewart [b,c,*]

[a] Department of Chemical & Biomolecular Engineering, University of Illinois at Urbana-Champaign, Urbana, IL 61801, USA
[b] Veterinary Clinical Medicine, University of Illinois at Urbana-Champaign, 1008 W. Hazelwood Dr., Urbana, IL 61802, USA
[c] Beckman Institute, University of Illinois at Urbana-Champaign, Urbana, IL 61801, USA

ARTICLE INFO

Article history:
Received 24 August 2009
Received in revised form 11 December 2009
Accepted 24 December 2009
Available online 4 January 2010

Keywords:
Microtopography
Tenocytes
Collagen
Tendon regeneration

ABSTRACT

This paper investigates the role of microtopographical features on the cytomorphology, alignment, proliferation and gene expression of tenocytes. We made use of simple microfabrication approaches to create surfaces patterned with topographical features suitable for in vitro studies of tenocytes. These surfaces were composed of glass substrates patterned with polymeric ridges spaced from 50 to 250 μm apart. Our studies demonstrate that the microgrooves differentially impact tenocyte shape, alignment and matrix organization along the direction of grooves. Groove widths significantly influenced cellular alignment, with 50 μm grooved patterns affecting alignment most substantially. Polarized light microscopy demonstrated that mature collagen fibers were denser and more oriented within 50 μm patterns. None of the patterns had a significant effect on the expression of genes linked to proliferation or extracellular matrix synthesis, although time in culture profoundly influenced both gene groups. COMP mRNA expression was moderately increased in tenocytes seeded onto 250 μm grooves, but there was no overall beneficial phenotypic effect of aligned growth. The results of this study indicate that microtopography affects cell density and alignment of tenocytes and leads to the deposition of an aligned collagen matrix, but does not significantly impact matrix gene expression or cell phenotype. These outcomes provide insights into the biology of tendon regeneration, thus providing guidance in the design of clinical procedures for tendon repair.

1. Introduction

Tendons are highly specialized connective tissues that connect muscles to bone and transmit the tensile loads that move and stabilize joints. Tendon damage that occurs through repetitive strain or acute trauma is a major problem for the orthopedic biomedical community. Damaged tendons have a very limited capacity for regeneration, since these tissues are relatively avascular and sparsely populated with cells of low mitotic activity [1]. The ability of tendons to transmit tensile loads without structural failure is a consequence of the highly ordered arrangement of collagen fibers, aligned along the vector of primary load. When tendons are damaged, the resultant scar tissue is of inferior mechanical strength and elasticity. Conservative approaches to the treatment of tendon strain are currently focused on minimizing the acute inflammatory phase of repair and consequent scar deposition, with rehabilitation programs designed to optimize scar fiber orientation. Surgical treatments aim to stimulate vascular ingrowth and tissue repair, reduce peritendinous adhesion formation and restore tendon–bone continuity [2]. These current therapies do not reliably restore an optimally organized tissue for tensile load-bearing. Tendon tissue engineering offers a promising alternative to regenerate damaged tendons. However, the factors that have the ability to stimulate tendon repair have not been identified.

Controlling cell–substrate interactions is critical to developing successful tissue engineering strategies. Recent advances in lithographic methods for microfabrication have facilitated substrate patterning and modification for cell studies. Researchers have studied the effect of surface topography [3,4], surface crystallinity [5], hydrophobicity [6], surface roughness [7] and chemical composition [8] on cellular responses. Cell substrate interactions have been studied in the context of patterned surface substrates for many cell types: fibroblasts [9–11], BHK cells [12,13], neuronal cells [14], Schwann cells [15–17], macrophages [18], epithelial cells [19], endothelial cells [20] and smooth muscle cells [21,22].

To date, the majority of studies addressing tendon tissue engineering have focused on developing biocompatible polymeric scaffolds for the directed migration of endogenous reparative cell populations [23,24] or ex vivo colonization of isolated cells prior to surgical implantation [25–27]. Mechanical loading is required

* Corresponding author. Tel.: +1 217 265 5206; fax: +1 217 244 1475.
E-mail address: matt1@illinois.edu (M.C. Stewart).
[1] These authors contributed equally to this work.

1742-7061/$ - see front matter © 2009 Acta Materialia Inc. Published by Elsevier Ltd. All rights reserved.
doi:10.1016/j.actbio.2009.12.047

for tenocyte homeostasis [28,29] and also impacts intrinsic tendon repair [30,31]. Biomechanical stimuli undoubtedly have an influence on the performance of any tissue-engineered tendon construct, but successful tendon regeneration requires a comprehensive understanding of the fundamental biological issues governing tenocyte growth and matrix orientation.

Tenocyte alignment and appropriate orientation of newly synthesized matrix are critical for tendon function [23,32]. However, the stimuli that influence the alignment of cells and the extent to which these factors affect tenocyte behavior are not yet well understood. In this work, we addressed the role of microtopographical factors on the alignment and growth of tenocytes. We fabricated substrates with groove widths ranging from 50 to 250 μm. These patterned substrates were used to investigate the influence of physical cues on the proliferation, cytomorphology, alignment and gene expression of tenocytes.

2. Materials and methods

2.1. Micropatterned substrate fabrication

Glass slides, 25 mm × 75 mm × 1 mm (Fisher Scientific, Pittsburgh, PA), were used as substrates for the fabrication of micropatterned structures. The slides were cleaned in piranha solution (H_2SO_4:H_2O_2 (30%) = 3:1) overnight, and subsequently rinsed with distilled water and dried in nitrogen. This was followed by sonication in isopropanol and acetone for 5 min each. After drying with nitrogen, the slides were exposed to oxygen plasma (100 torr, 100 W power) for 1 min. The micropatterned substrates were fabricated on the cleaned glass slides using standard photolithographic procedures. SU-8 5 photoresist (Microchem, Newton, MA) was spin-coated on the glass slides at 1000 rpm for 30 s. SU-8 is a biocompatible photoresist obtained by dissolving a polymeric epoxy resin (glycidyl ether of bisphenol A) in an organic solvent (gamma-butyrolactone) and adding a photoacid generator taken from the family of the triarylium–sulfonium salts [33]. The substrates were soft-baked at 65 °C for 2 min, followed by baking at 95 °C for 5 min. Transparency masks (CAD/Art services, Bandon, OR) of the pattern were placed on the glass substrates and exposed to UV light using a mask aligner (Suss Microtech MJB3) for 12 s (power = 334 MW). The substrates were then subjected to a two-step post-exposure bake: 1 min at 65 °C followed by 2 min at 95 °C. The patterns were developed in a propylene glycol monomethyl ether acetate solution (Sigma–Aldrich, St. Louis, MO) by dissolving the unexposed portions of the photoresist. After drying the substrates with nitrogen, they were exposed to UV light without a mask and hard baked at 150 °C on a hotplate overnight, to ensure complete polymerization of SU-8 and enhance its adhesion to the glass. The micropatterned slides were sterilized with hydrogen peroxide before use in cell culture experiments and were treated with oxygen plasma to promote cell adhesion. A schematic illustration of the micropatterned substrate is shown in Fig. 1a, along with a high-resolution of a 50 μm pattern (Fig. 1b). The grooves of the micropatterns were free from photoresist all the way down to the glass.

2.2. Tenocyte isolation and culture

Superficial digital flexor tendon specimens were collected from four adult horses that were euthanized for reasons not associated with musculoskeletal disease. These horses were euthanized in accordance with approved IACUC protocols by an intravenous overdose of a barbiturate anesthetic agent. The tendon specimens were diced and digested with trypsin–ethylenediaminetetraacetic acid for 1 h (Invitrogen, Carlsbad, CA) followed by overnight digestion in 0.15% collagenase II (Worthington, Lakewood, NJ). The trypsin and collagenase digestions were carried out in a 37 °C shaking incubator. Following overnight incubation, the digest suspension was passed through a 40 μm pore-size filter to remove incompletely digested tissues. The released cells were pelleted by centrifugation at 390*g* for 10 min and washed twice in phosphate-buffered saline (PBS; HyClone, Logan, UT). The cells were counted using a hematocytometer and cryo-stored in freezing medium containing 50% high glucose Dulbecco's modified Eagle's medium (DMEM) (HyClone, Logan, UT), 40% fetal bovine serum (Gemini Bio-Products, West Sacramento, CA) and 10% dimethylsulfoxide (Fisher Scientific, Rochester, NY) in liquid nitrogen.

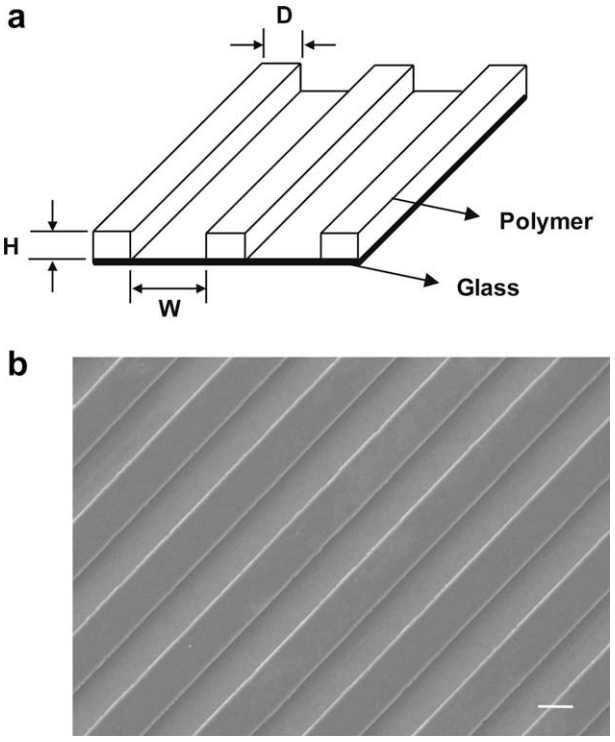

Fig. 1. (a) Schematic illustration of micropattterned substrates with critical dimensions: groove width (W), 50, 100 and 250 μm; ridge width (D), 50 μm; and ridge height (H), 15 μm. (b) Scanning electron micrograph image of a 50 μm grooved micropatterned substrate. Scale bar: 50 μm.

2.3. Tenocyte seeding onto the patterned surfaces

The tenocytes were thawed, counted and seeded in 55 cm^2 culture dishes (Corning Incorporated, Corning, NY) at a density of 5×10^4 cells cm^{-2}. They were cultured in high glucose DMEM, supplemented with 10% fetal bovine serum, L-glutamine (2 mM) (Invitrogen, Carlsbad, CA), penicillin G sodium (100 U ml^{-1}), streptomycin (100 μg ml^{-1}) (Invitrogen, Carlsbad, CA), amphotericin B (2.5 μg ml^{-1}) (MP Biomedicals, Solon, OH) and ascorbic acid (50 μg ml^{-1}) (Wako, Richmond, VA) until confluence. The cells were then trypsinized and seeded onto the patterned surfaces at an initial density of 5×10^4 cells cm^{-2} in four-well rectangular dishes (Thermo Fisher Scientific, Rochester, NY) and cultured under 5% CO_2 at 37 °C for up to 72 h. The seeding density calculations were based on the surface areas of the microgroove floors available for cell attachment. Caution was taken to ensure that cells were not seeded in clumps thus ensuring uniform distribution. In each experiment, 10 replicates were seeded for each micropatterned substrate and time point: two patterns for confocal microscopy, two for SEM, two for optical microscopy and four patterns for RNA isolation.

Optical microscopic images of the cells were acquired with a Nikon Eclipse TS 100 inverted microscope on days 1, 2 and 3 after seeding. The day 1 image acquisition occurred between 16 and 20 h after seeding, before any substantial cell division could occur. Samples were collected for gene expression analyses at 36 and 72 h. In addition, slides were placed in 10% buffered formalin (Fisher Scientific, Rochester, NY) for fluorescent confocal analyses of cell density and cytoskeletal organization. These slides were collected at 16 h after seeding, prior to any cell proliferation, at the mid-point of the study (36 h) and at the termination of study (72 h).

2.4. Confocal and fluorescent imaging

The formalin-fixed slides were washed three times with PBS. The cells were then permeabilized with 0.1% Triton X-100 (Sigma–Aldrich, St. Louis, MO) at room temperature for 5 min and washed again in PBS. The slides were blocked with 0.1% bovine serum albumin (Sigma–Aldrich, St. Louis, MO) in PBS for 20 min to prevent non-specific binding. Alexa Fluor® 488 phalloidin (Invitrogen, Carlsbad, CA) was reconstituted in methanol, diluted in PBS to 5 U ml^{-1} and applied to the slides for 20 min. The slides were rinsed in PBS, exposed to 0.1 μg ml^{-1} of 4′,6-diamidino-2-phenylindole (DAPI) in PBS (Invitrogen, Carlsbad, CA) for 1 min, washed in PBS and coverslip-mounted using an aqueous mounting medium (R&D Systems Inc., Minneapolis, MN). Cells were imaged with a Leica TCS SP2 multiphoton confocal laser scanning microscope (Leica Microsystems, Germany). The images were acquired with 10× (0.4 NA), 40× (1.25 NA) and 63× (1.32 NA) objectives. The Alexa 488 dye was excited using the 488 line of an argon laser. DAPI fluorescence was detected under the two-photon excitation with a 785 nm pulse laser line (Ti:Sapphire, 100 fs, 80 MHz). Polarized light microscopy was used to image collagen fibril deposition and organization in formalin-fixed specimens, using a Leica DM 2000 light microscope and polarizing lens. Images are acquired using a Leica DFC320 digital camera.

2.5. Cell density calculations

The fluorescent confocal images of cell layers were used for cell density calculations. DAPI-stained cell nuclei were counted in 20 randomly selected 12,500 μm^2 regions of interest (ROIs) across the floors of the micropatterned grooves. Cell densities were extrapolated from an average of the nuclear counts per ROI area.

2.6. Quantitative analyses of cell shape and alignment

Images of the tenocytes cultured on micropatterned surfaces were quantitatively analyzed using ImageJ software (free download available at http://rsbweb.nih.gov/ij/). Briefly, the images acquired from optical microscope were converted to 8-bit grey scale and thresholded to distinguish cellular outlines from the non-cellular background signal. Thus, the program detected cells on the basis of contrast and fitted the cellular outlines to equivalent ellipses [22,34]. Areas smaller than the area of a cell were excluded while fitting the ellipses. The following cell shape characteristics were measured for each fitted ellipse: major axis, minor axis, aspect ratio (major axis/minor axis), perimeter, area and orientation angle with respect to the direction of grooves. The major axis was taken as the direction of angle of orientation of the cells. The angle of the micropattern was measured for each image and added or subtracted from the orientation angle of the tenocytes to get an accurate value for the orientation of cells with respect to the grooves. The angle for each cell was converted such that 0° represented cell orientation along the direction of the microgroove and 90° represented a perpendicular orientation with respect to the direction of the grooves. The data for each image were transferred into Excel (Microsoft, Seattle, WA) for further analysis. For more detailed evaluation of cell orientation in the 250 μm microgrooves, the substrate surface was segregated into "edge" zones within 50 μm of the groove wall, "mid" zones positioned between 50 and 100 μm from the groove walls and "central" zones located in the central 50 μm of the microgrooves.

Cell morphology was quantified using cell shape index (CSI), defined as $(4\pi \times \text{cell area})/(\text{cell perimeter squared})$. The cell shape index is a measure of cell roundness, with "1" representing a perfect circle and "0" a straight line. The cellular contours were identified and analyzed for all non-overlapping cells in this manner. In cases where confluent cell layers prevented automated assessment due to cell–cell contact, cellular outlines were manually drawn using a Graphire Pen Tablet (Wacom Technology Corporation, Vancouver, WA) and orientation angles and other variables were measured for each cell individually using ImageJ. Cells that overlapped or aggregated together or wherever boundaries of contacting cells could not be distinguished clearly were not used for quantitative analysis. Two hundred cells were used for quantitative analysis for each micropattern for each time point.

2.7. Gene expression analyses

Gene expression analyses were carried out using tenocytes isolated from four donors, to determine whether microtopographical cues influence the transcription of genes associated with proliferation, matrix synthesis or the tenocytic phenotype. To this end, we compared gene expression of tenocytes seeded on substrates with 50 μm microgrooves and 250 μm microgrooves, to reflect tightly constrained and unconstrained attachment conditions, respectively. Gene expression was assessed at the mid-point (36 h) and the termination (72 h) of the study. Total RNA was extracted from tenocytes using Trizol® (Invitrogen, Carlsbad, CA), following the manufacturer's instructions. Northern blot analyses were carried out using previously described protocols [35,36] to assess the expression of the following strongly expressed genes: collagen type I, proliferating cell nuclear antigen (PCNA) and elongation factor 1-α (EF1-α). The primers used to generate the cDNA probes are listed in Table 1. Briefly, 4 μg of total RNA was electrophoresed through an agarose–formaldehyde gel. After a 2–3 h separation, the ribosomal RNA bands were stained with ethidium bromide to assess equivalence of loading and RNA integrity. The RNA was then transferred to a charged nylon membrane (GE Osmonics Labstore, Minnetonka, MN) by high-salt capillary transfer and cross-linked by UV light. The membranes were rinsed in 5× SSPE and pre-hybridized with a hybridization solution containing 5× SSPE, 5× Denhardts' solution (Eppendorf, Westbury, NY), 0.5% SDS (Fisher Scientific, Rochester, NY), 10% dextran sulfate (Molecular weight 5×10^5) (Fisher Scientific, Rochester, NY) and 150 μg ml^{-1} of denatured salmon sperm DNA (Invitrogen, Carlsbad, CA) for one hour. The probes were radiolabeled with dCTP ^{32}P (Amersham, Piscataway, NJ) using Prime-It® II Random Primer Labeling Kit (Stratagene, Cedar Creek, TX) following the manufacturer's instructions, denatured and then added to tubes containing the membranes that had been pre-hybridized. After overnight hybridization, the membranes were washed in 2× SSPE containing 0.5% SDS. Sequential washes were done until the washing solution reached 0.5× SSPE with 0.125% SDS. The membranes were wrapped in plastic and placed into a lightproof cassette with radiograph film and stored at −80 °C during exposure. The radiograph film was developed after 1–4 days of exposure, depending on the target mRNA abundance and probe activity.

Quantitative PCR (qPCR) was simultaneously used to compare expression profiles of tenocytes seeded onto 50 and 250 μm substrates, representing constrained and unconstrained conditions, respectively. Expression patterns of the extracellular matrix

Table 1
PCR primers utilized for cDNA probe production and qPCR reactions.

mRNA	Sense primer	Anti-sense primer	Size (bp)
Cyclin D1	5′CATGAACTACCTGGACCGCTT	5′TCGAAGGACAGGAAGTTGTT	438
Cyclin A2	5′TGGAAGATGAAAAGCCAGTGA	5′GAGGTAGCTCTGGTGAAGGTC	704
PCNA	5′GTGTAAACCTGCAGAGCATG	5′GGAATTCCAAGTTGTTCAAC	285
Coll I	5′AGCCAGCAGATCGAGAACAT	5′CGCCATACTCGAACTGGAAT	303
Coll III	5′AGGGGACCTGGTTACTGCTT	5′TCTCTGGGTTGGGACAGTCT	215
Aggrecan	5′GACGCCGAGAGCAGGTGT	5′AAGAAGTTGTCGGGCTGGTT	201
COMP	5′TCATGTGGAAGCAGATGGAG	5′TAGGAACCAGCGGTAGGATG	224
Tendin	5′CCCTCAAGTGAAGGTGGAGA	5′GTTGCAAGGCATGATGACAC	149
EF1-α	5′CCCGGACACAGAGACTTCAT	5′AGCATGTTGTCACCATTCCA	329

genes collagen type I, type III and aggrecan, the phenotypic markers cartilage oligomeric matrix protein (COMP) and Tendin, the proliferation markers PCNA, cyclin D1 and cyclin A, and the reference gene elongation factor 1-α (EF1-α) were assessed in these experiments. One microgram of total RNA from each sample was converted to cDNA using oligo T primers and the Superscript II reverse transcription kit (Invitrogen, Carlsbad, CA) as per the manufacturer's instructions. The samples were run in duplicate and each reaction (25 μl) contained 12.5 μl of SYBR® GreenER™ qPCR super mix (Invitrogen), 10 pmol of sense and anti-sense primers (Sigma–Aldrich, St. Louis, MO) and 25 ng cDNA. SYBR Green fluorescence was measured using a Bio-Rad "iCycler" thermal cycler (Bio-Rad Laboratories, Hercules, CA). The expression data in each experiment were normalized to expression of the reference gene, EF1-α. For each target gene, relative mRNA levels were converted to fold changes in expression relative to expression in the 50 μm–36 h samples. As an example, if the mean expression of the target gene at 72 h was twice that of the 50 μm–36 h measurement, the fold-increase would be designated as "2".

2.8. Statistical analyses

Statistical differences between cell densities and cell shape indices were analyzed by two-way analysis of variance (ANOVA) ($p < 0.05$). Dunnett's or Bonferroni's post hoc test were used as required to identify significant differences between specific data sets. The Kolmogorov–Smirnov test was used to assess the significance of differential alignment behaviors of tenocytes on the substrates ($p < 0.05$). qPCR data were also analyzed by two-way ANOVA ($p < 0.05$), using data sets from four replicate experiments.

3. Results

Preliminary experiments were carried out using micropatterned substrates with groove widths ranging from 20 to 500 μm, to identify biologically informative microgroove dimensions. Tenocytes seeded onto substrates with 20 μm grooves were not able to attach efficiently, while cell monolayers seeded onto microgrooves 250 μm or wider closely resembled unconstrained monolayers. Therefore, subsequent experiments focused on the differential behavior of tenocytes on substrates with 50 m and 250 μm wide microgrooves, representing highly constrained and unconstrained seeding conditions, respectively. In some experiments, 100 μm wide microgrooved substrates were included to represent an intermediate degree of confinement. The control slides comprised an unpatterned glass surface providing a completely unrestricted environment for cell growth and proliferation. Cell attachment was also assessed on SU-8 surfaces. SU-8 has been used as a patterning material in substrates in fabrication of bioreactors and is non-cytotoxic [37]. Successful cell attachment, growth and proliferation on SU-8 patterned surfaces demonstrated the biocompatibility of SU-8 photoresist.

3.1. Effects of microgroove width on cell density

Tenocytes were seeded at an initial density of 5×10^4 cells cm^{-2} onto 50, 100 and 250 μm wide microgrooves or onto an unpatterned substrate. The seeding densities were calculated on the basis of the groove "floor" areas only and were selected to provide for approximately two cell doublings on each surface prior to confluence. At the first assessment point, within the first day of seeding and prior to any significant proliferative activity, no changes in cell density were observed (Fig. 2). By 36 h the growth curves had diverged, and there were significant differences in cell densities between all four substrate groups by 72 h (Fig. 2). The cell densities at confluence reflected the degree of constraint. Accepting the statistical outcomes, it was apparent that the cell density at confluence in the 50 μm grooves was substantially less (approximately half) than those of the other three substrates.

3.2. Effects of microgroove width on cell shape

Quantitative analyses of tenocyte shape after seeding onto confined (50 μm) or unconfined (250 μm) microgrooves demonstrated that both populations became progressively and significantly more fusiform (long and narrow) over time, as the cells reached confluence (Fig. 3). Prior to confluence, 1 and 2 days after seeding, the tenocytes seeded under constrained conditions (50 μm) were significantly more fusiform than unconstrained cells (250 μm). However, by day 3, once cell density peaked, the cell shape indices were highly similar. As seen in Fig. 4a and b, the majority of cells in each group adopted a fusiform morphology (see also Fig. 5a–d).

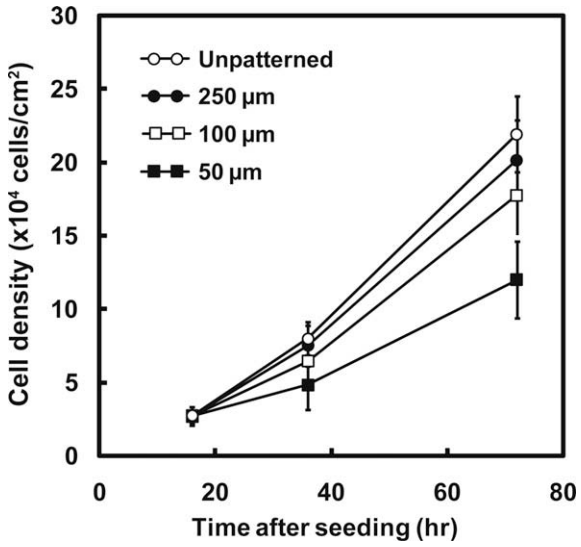

Fig. 2. Cell density as a function of time after seeding. By 72 h, each group was statistically significantly different from the others ($n = 20$; $p < 0.05$).

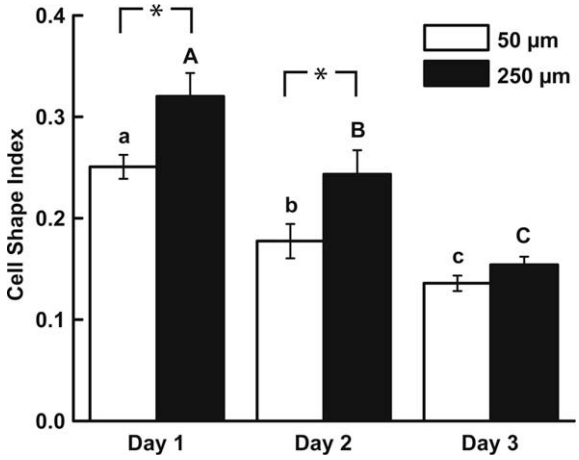

Fig. 3. Cell shape index as a function of time after seeding. a, b and c indicate statistically significant differences between cell shape indices across time on 50 µm patterned substrates. Similarly, A, B and C indicate statistically significant differences across time on 250 µm patterned substrates. Asterisks denote statistically significant differences between the substrate groups at each time point ($n = 30$; $p < 0.05$).

However, this morphology was consistent (Fig. 4c) under confined conditions (50 µm), whereas the unconstrained conditions provided by 250 µm microgrooves accommodated a small number of comparatively stellate cells prior to confluence (Fig. 4d).

3.3. Effects of microgroove width on cell alignment

Microgroove width exerted a profound effect on cell alignment. As expected, tenocytes seeded onto 50 µm microgrooves were aligned within 30° of the microgroove orientation soon after seeding (Fig. 5a and e). The cells on unpatterned surfaces exhibited an essentially random orientation, while tenocytes seeded onto 100 and 250 µm microgrooves showed intermediate alignment (Fig. 5b–g). After 3 days in culture, the alignment of tenocytes seeded onto 50 µm microgrooves was more focused along the orientation of the grooves, with 50% of the population aligned within 5° of the groove axis and the entire population constrained within 20° of this vector (Fig. 5g). As the cell layers reached confluence, the tenocyte alignment distribution within the 100 µm microgrooves closely approximated that of the 50 µm group (Fig. 5f and g). Cell alignment on the unpatterned surfaces remained random, while the cells seeded onto 250 µm microgrooves displayed an intermediate level of orientation, with 50% of the cells aligned within 20° of the groove axis (Fig. 5g). This outcome was driven, to a large extent, by the edge effect exerted on the confluent cell layers by the groove walls. Cells adjacent to groove walls ("edge" zone) were aligned as a result of guidance provided by the walls, whereas cells positioned in the "mid" and "central" zones of the groove were significantly less aligned to the longitudinal axis of the groove (Fig. 6). "Central" zone cells were, in effect, randomly aligned, as was evident on the unpatterned surfaces (Figs. 5g and 6b).

3.4. Effects of microgroove width on collagen alignment

The alignment of secreted collagen was assessed using polarized light microscopy. The birefringence of collagen secreted by tenocytes seeded onto 50 µm microgrooves (Fig. 7b) was noticeably stronger (pink/orange bands) than the signals detected from unseeded microgrooves (Fig. 7a) or from tenocytes on 250 µm substrates (Fig. 7c) and appeared to be organized in a sinusoidal pattern, bounded by the groove edges. In contrast, the samples with 250 µm microgrooves exhibited little or no collagen fiber birefringence.

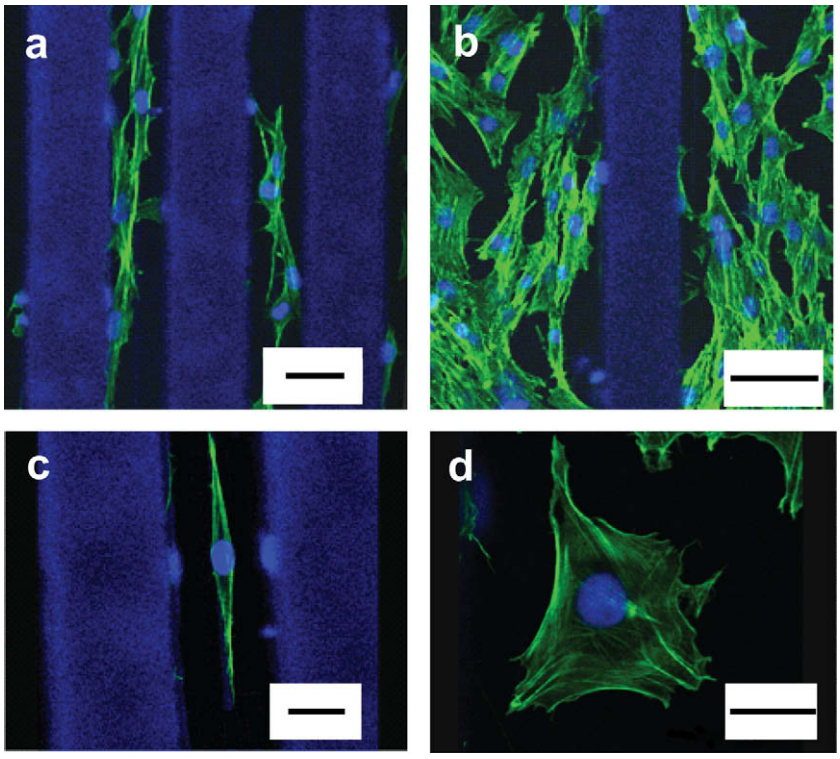

Fig. 4. Confocal images of tenocytes growing on 50 µm (a and c) and 250 µm (b and d) micropatterned substrates. Polymeric actin is localized with phalloidin (green), while cell nuclei are localized with DAPI (blue). Tenocyte monolayers 36 h after seeding onto grooves of widths of (a) 50 µm and (b) 250 µm. Higher power images of individual cells seeded onto (c) 50 µm and (d) 250 µm substrates. Scale bar: 50 µm.

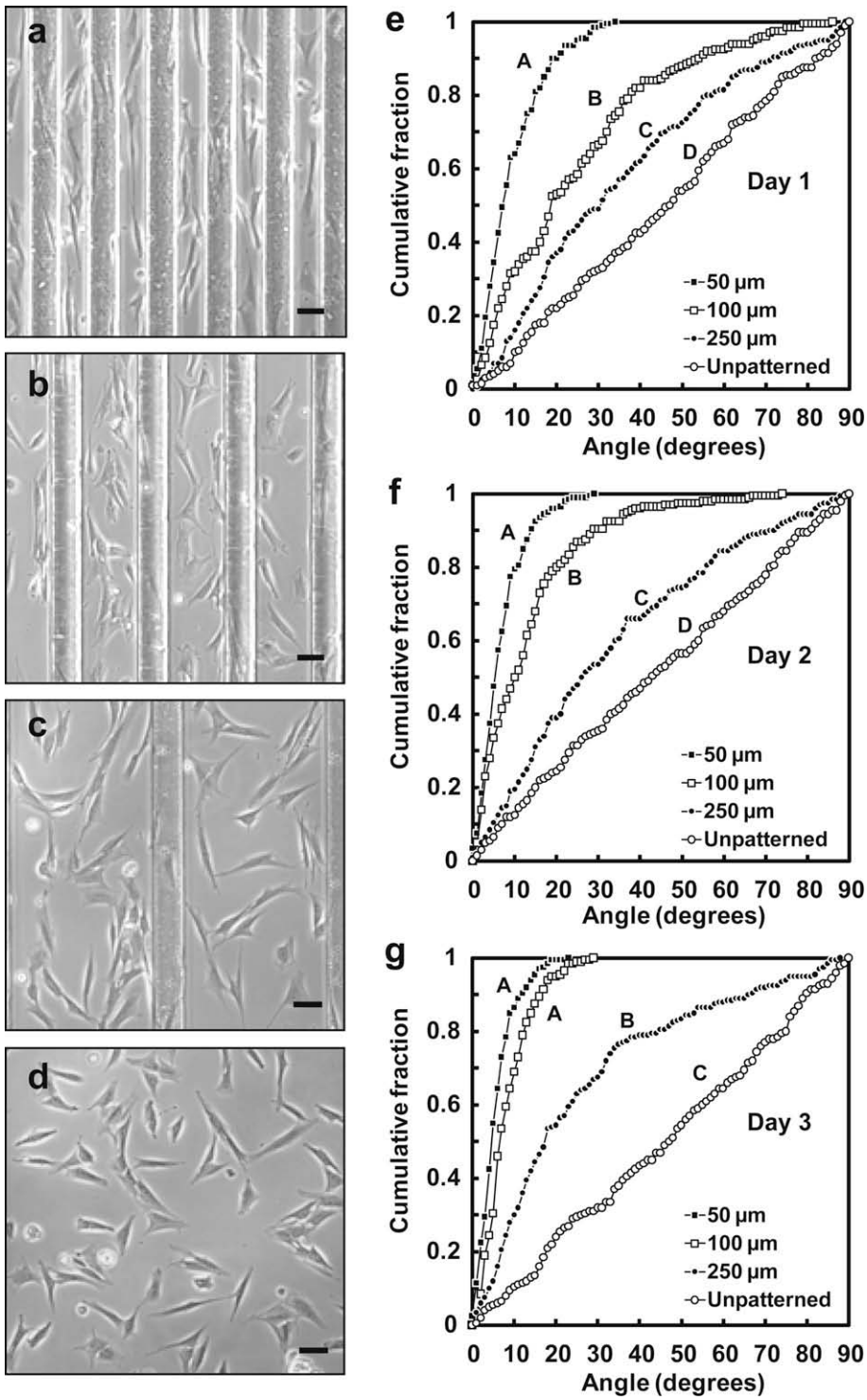

Fig. 5. Alignment of tenocytes on micropatterned substrates. Images show representative tenocyte orientations in grooves of widths (a) 50 µm, (b) 100 µm and (c) 250 µm and on (d) unpatterned control slides on day 1. Scale bar: 50 µm. Plots show the cumulative angular distribution fractions of tenocytes (*y*-axis) in 1° bins (*y*-axis) (e) 1, (f) 2 and (g) 3 days after seeding. In all cases, 0° corresponds to the direction along the grooves. The plots are based on measurements using 200 cells for each substrate pattern at each time point. In each plot, significantly different curves are designated by distinct letters (A, B, C or D).

3.5. Effects of microgroove width on gene expression

The gene expression analyses focused on the differential effects of 50 m and 250 µm patterned substrates on tenocytes and are presented in Table 2. Time in culture exerted significant but opposite effects on the expression of genes associated with cell proliferation (Fig. 8 and Table 2) and extracellular matrix synthesis. Expression of PCNA (Fig. 8), cyclin D1 and cyclin A2 (Table 2) fell significantly between days 1 and 3, indicative of transient proliferative activity prior to the cell layers reaching confluence. In contrast, expression of collagen types I (Fig. 8) and III and aggrecan (Table 2) increased in the later stages of culture, although considerable inter-experimental variability in aggrecan expression precluded a statistically significant result in this study. The influence of substrate groove

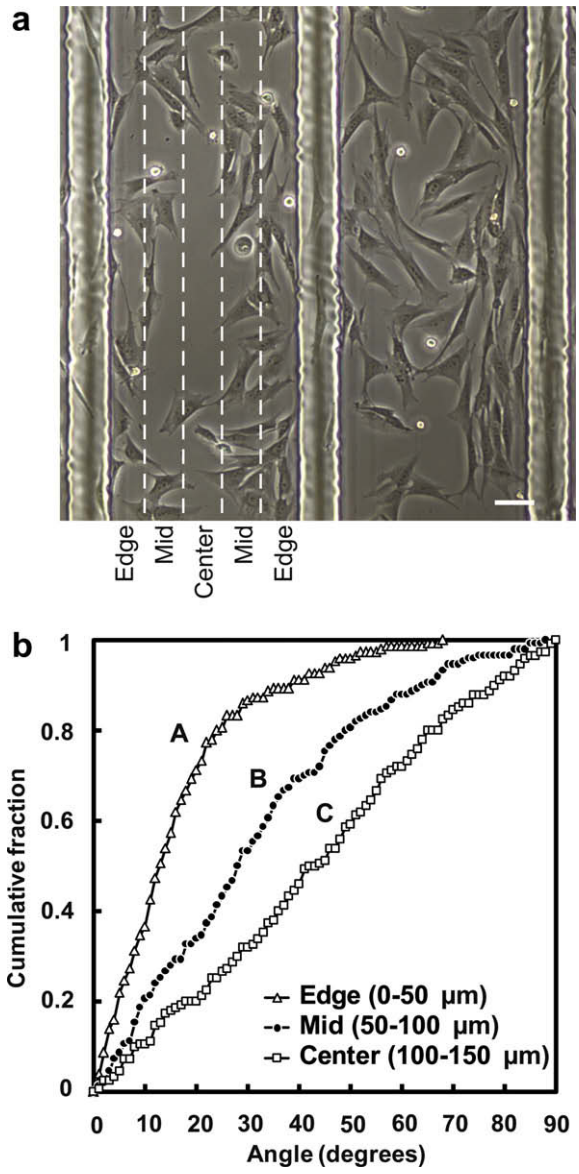

Fig. 6. (a) Angular distribution of tenocytes as a function of distance from groove wall. The region within each 250 μm width micropatterned groove is divided into three zones transversely in order to determine the edge effects: "edge" (0–50 μm from groove wall), "mid" (50–100 μm) and "central" (100–150 μm) regions. (b) The distribution plot shows the cumulative angular distribution fractions of tenocytes (y-axis) in 1° bins (x-axis) within each zone 1 day after seeding. The plots are based on measurements using 150 cells for each zone in a 250 μm wide substrate pattern. The significantly different curves are designated by distinct letters (A, B or C). Scale bar: 50 μm.

width on expression of the tenogenic markers Tendin and COMP was not marked. Tendin mRNA levels fell moderately over time, while COMP expression was increased by approximately 50% in the 250 μm group.

4. Discussion

4.1. Cell shape characteristics on topographically patterned substrates

The effect of topographical patterning on tenocyte shape was studied quantitatively and qualitatively using static optical micrographs and confocal images. Accepting that the cell shape indices of tenocytes seeded onto 50 μm substrates were statistically lower than cells growing in 250 μm grooves after 1 and 2 days in culture, reflecting a more fusiform morphology, this effect was not marked. The quantitative differences at these times amounted to less than 10% of the total index that encompasses cell shapes ranging from circles (1.0) to virtual lines (0.0). The tenocytes were predominantly fusiform on both substrates, and this morphology was progressively reinforced over time, as the cell layers became confluent. By day 3, the cell shape indices were essentially identical (Fig. 3).

Although it was not subject to quantitative assessment, the fluorescent, confocal images of tenocytes in Fig. 4a–d demonstrate that substrate microtopography also affected nuclear profiles. The nuclei of cells seeded onto 50 μm microgrooves were more ovoid than those of cells seeded under unconstrained conditions. This feature is particularly evident in the "single cell" images in Fig. 4c and d. Nuclear deformation has been linked to alterations in tenocyte signal transduction [38] and constitutes a potential mechanism by which substrate microtopography might influence tenocyte behavior independently of direct cellular orientation or growth constraints.

4.2. Effects of microtopography on tenocyte alignment

Microgroove widths significantly influenced tenocyte alignment, consistent with the outcomes of a number of other studies that addressed cell–topography interactions using cells of neuronal, epithelial and myoblastic lineages [12,39–43]. The impact of microgroove width was evident within the first day of seeding. Approximately 65% of tenocytes seeded onto 50 μm microgrooves were aligned within 10° of the groove axis and 90% were within 20° of the axis at the first assessment. The degree of alignment increased over time; almost all cells in 50 and 100 μm grooves were aligned along the channel axis after 72 h of seeding.

In contrast to the tenocytes seeded onto 50 and 100 μm grooves, the cells seeded onto 250 μm grooves exhibited near-random orientation (Fig. 5f). Accepting this, it was apparent that tenocytes growing under essentially unconstrained conditions developed locally aligned cell clusters at confluence, although there was no overall alignment of the cell population. This observation, along with the progressive orientation that occurred in the 50 and 100 μm-confined tenocytes over time (Fig. 5e and f), suggest that intercellular interactions play a role in positioning individual cells, independently of any constraints imposed by substrate geometries.

Not surprisingly, the microgroove walls exerted a considerable local effect on tencocyte alignment. This was evident immediately in the 50 μm microgroove populations and became progressively more influential in the 100 and 250 μm cultures over time (Fig. 5e–g). In effect, cells positioned directly along the microgroove walls applied an alignment cue to adjacent cells as the monolayers reached confluence. This phenomenon was responsible for the late-stage quantitative differences between the tenocyte populations seeded onto 250 μm grooves and those seeded onto unpatterned surfaces (Fig. 5g), and was clearly evident in the analyses of cell alignment in the "edge", "mid" and "central" regions of the 250 μm grooves (Fig. 6). The critical effects of substrate interfaces on cell behavior have been recognized in a number of other studies [17,39] and represent an additional mechanism to influence cell alignment, independent of other substrate geometries.

In recent years, a number of promising technologies have been developed to address tissue engineering applications of highly anisotropic tissues, such as tendon, ligament and peripheral nerves [44,45]. In these tissues, cell orientation and the associated matrix alignment are critical for subsequent function. In particular, surface lithographic and electrospinning techniques have been used to generate highly oriented scaffolds, where scaffold nanotopographies are considerably less than cellular dimensions [24,41,44,46]. The phenotypic consequences of substrate-mediated cellular alignment have varied considerably between studies, as summarized in

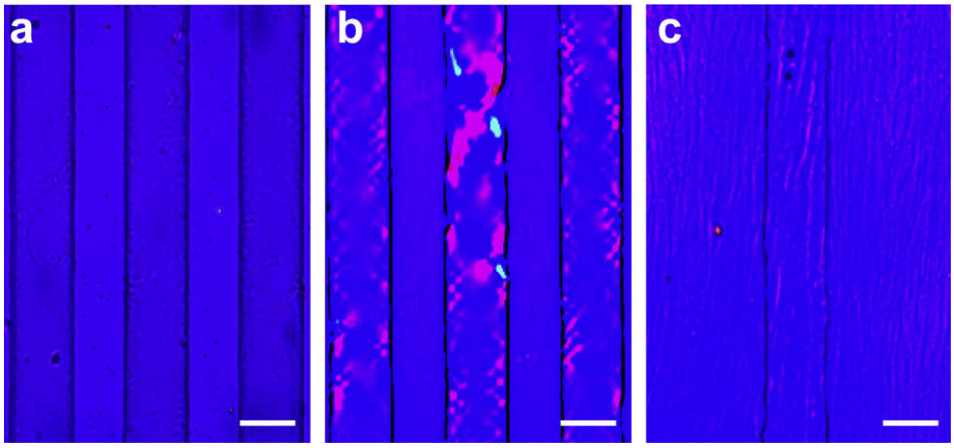

Fig. 7. Polarized light microscopic images of (a) an unseeded 50 μm wide patterned substrate and of collagen secreted by tenocytes seeded onto (b) 50 μm and (c) 250 μm wide patterned substrates after 72 h. Scale bar: 50 μm.

Table 2
Results of tenocyte gene expression analyses.[a]

	36 h		72 h		*p* values	
	50 μm	250 μm	50 μm	250 μm	Time	Width
Proliferation markers						
Cyclin D1	1.01 ± 0.172	0.64 ± 0.227	0.07 ± 0.014	0.42 ± 0.246	0.0002	0.7527
Cyclin A2	1.01 ± 0.172	0.91 ± 0.260	0.09 ± 0.031	0.14 ± 0.120	<0.0001	0.8251
PCNA	1.00 ± 0.072	1.34 ± 0.348	0.21 ± 0.066	0.19 ± 0.022	<0.0001	0.1243
ECM genes						
Coll I	1.01 ± 0.154	0.79 ± 0.08	1.91 ± 0.23	2.39 ± 0.90	0.0002	0.5936
Coll III	1.01 ± 0.128	1.13 ± 0.052	2.04 ± 0.167	1.97 ± 0.219	<0.0001	0.7095
Aggrecan	1.09 ± 0.523	0.75 ± 0.196	0.81 ± 0.384	2.86 ± 2.028	0.1113	0.1389
Tenogenic genes						
Tendin	1.02 ± 0.206	1.12 ± 0.109	0.9 ± 0.024	0.74 ± 0.095	0.0023	0.6126
COMP	1.01 ± 0.146	1.12 ± 0.125	1.20 ± 0.156	1.61 ± 0.265	0.0025	0.0136

[a] In each experiment, the level of expression of the genes listed in this table was normalized to the expression of the reference gene, EF1-α. For each gene, relative mRNA levels are presented as fold changes in expression relative to expression in the 50 μm–36 h samples in each experiment. Values are mean ± standard deviation; $n = 4$.

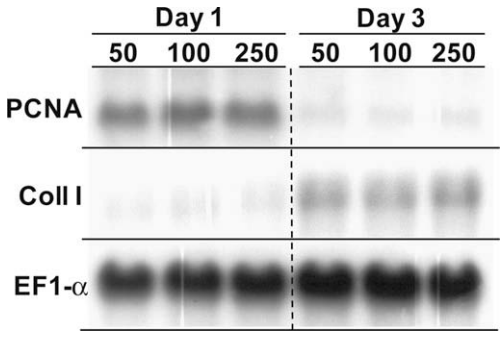

Fig. 8. Northern blot of proliferating cell nuclear antigen (PCNA), collagen type I (Coll I) and elongation factor 1-α EF1-α) expression by tenocytes cultured on 50, 100 and 250 μm patterned substrates for 1 and 3 days.

a review by Martinez et al. [47]. The results of our study indicate that tenocyte alignment can be induced by topographic constraints that are significantly larger than individual cellular dimensions, consistent with the findings of other studies [48]. These physical cues can be easily incorporated into the surface topographies of solid-state planar scaffolds to regulate alignment of ex vivo-seeded cells or control orientation of reparative cells that colonize scaffolds following implantation. The pronounced "edge effect" observed at the periphery of the 250 μm microgrooves (Fig. 6) suggests that topographical cues, such as distinct surfaces or material interfaces, can exert a considerable effect on cells without explicitly requiring a confined groove.

4.3. Effects of microtopography on collagen orientation

Of particular importance to the issue of tendon regeneration, polarized light microscopic imaging of the extracellular matrix secreted by the tenocyte monolayers demonstrated a sinusoidal organization of collagen fibers (Fig. 7a) in the 50 μm-confined cultures. The periodicity of this organization (80–100 μm) approximates that of the collagen fiber "crimp" seen in equine flexor tendons [49] and rat tail tendons [50]. The matrices secreted by tenocytes maintained in 250 μm microgrooves showed no evidence of collagen alignment (Fig. 7b). The organization of tendon collagen provides the 3–5% tensile elasticity critical for the load-bearing function of mature tendons and is a structural requirement for effective functional regeneration of tendon tissue. The sinusoidal collagen fiber organization observed in the 50 μm microgrooves developed in the absence of any mechanical loading stimulus, apart from the intrinsic tension generated through cell adhesion to the underlying substrates. These data are consistent with similar experiments carried out with MC3T3-E1 osteoblast-like cells [51] and suggest that appropriate alignment of secreted collagen can occur as a consequence of primary cell orientation,

independent of load [52]. Additional experiments will be required to determine whether cell alignment and tensile loading exert synergistic effects on tenocyte matrix synthesis and organization.

4.4. Effects of microtopography on tenocyte gene expression

Overall, the gene expression analyses documented a time-dependent transition from a proliferative cell population to a growth-arrested, matrix-synthetic population, as evident in the time-dependent down-regulation of PCNA and cyclin expression and concurrent increases in matrix gene mRNA levels. Substrate microtopography had comparatively little influence on this transition, most likely reflecting the equal seeding densities at the start of each experiment (Fig. 2) and the subsequent impact of contact inhibition as the cell monolayers approached confluence.

The phenotypic responses of tenocytes to the micropatterned substrates were inconsistent. Tendin mRNA levels were down-regulated over time on both substrates, whereas COMP expression increased significantly with time in culture and was also more highly expressed in the unconstrained (250 μm) tenocyte cultures (Table 2). COMP acts to regulate collagen fibrillogenesis in load-bearing connective tissues [53], and COMP expression by tenocytes is stimulated by both mechanical and growth factor-mediated anabolic stimuli [54]. Increased COMP expression by tenocytes in the later stages of these experiments likely reflects the matrix-synthetic state of the cells at these times. Collectively, there was no indication that cell and collagen matrix alignment augmented expression of the tenocytic phenotype, consistent with recent findings of Charest et al. [43] in the context of myoblastic differentiation.

The effects of substrate topography cannot be separated completely from the effects due to patterned chemistry. The control experiments, however, revealed that less than 10% of cells preferred to attach to SU-8 ridges compared to glass microgrooves. Subsequently, the degree of confined environment controlled alignment of cells within the grooves. Therefore, the quantitative analysis presented here focused on influence of substrate dimensions on alignment response of cells and potential effects of surface chemistry were not considered. In future work, it would be instructive to compare synergistic as well as competitive effects of surface chemistry and topography by using a chemically modified surface that shows comparable cell adhesion.

Design rules, such as those derived from the in vitro studies reported here, can be applied in the design of similar in vivo implants to improve tendon regeneration strategies [55]. Recent studies comparing conduits with microgrooved inner surfaces to smooth-surfaced conduits have shown that microgrooved surfaces can enhance peripheral nerve regeneration in vivo [45,56,57]. The results of the current study indicate that analogously designed conduits with optimum dimensions could be developed to improve tendon repair. Further, a number of additional factors can govern cell behavior and cell–substrate interactions, including substrate properties, presence of growth factors and mechanical loading. All of these have to be considered individually and collectively when designing scaffolds with implantable materials for in vivo studies. Our results provide a basis for geometric considerations in designing microgrooved scaffolds for tendon repair.

5. Conclusion

Micropatterned surfaces can direct the aligned growth of tenocytes. We demonstrated this phenomenon of contact guidance by microfabricated patterns created by simple photolithographic methods. After 3 days in culture, 99.5% of tenocytes were aligned within 20° of the direction of grooves in 50 μm micropatterns. Groove widths also significantly influenced cell shape and growth. The cells were more elongated and less dense at confluence in narrow grooves. The most significant finding was the influence of cell alignment on secreted collagen fiber alignment. Even in the absence of mechanical loading, collagen alignment was observed in correspondence with cellular alignment. Proliferative and matrix gene expression profiles were inversely affected by time in culture, and were minimally influenced by surface topography. Further, surface topography did not influence expression of the tenocytic phenotype markers, Tendin and COMP. In summary, microtopographical features can be optimally controlled to influence both tenocyte and extracellular collagen alignment for tissue engineering applications.

Acknowledgements

This work was funded by the Beckman Institute for Advanced Science and Technology, University of Illinois at Urbana-Champaign and the United States Equestrian Foundation. The microfabrication work was carried out in the Frederick Seitz Materials Research Laboratory Central Facilities, University of Illinois, which are partially supported by the US Department of Energy under Grant DEFG02-91-ER45439.

Appendix A. Figures with essential colour discrimination

Certain figures in this article, particularly Figures 1, 5, 6 and 8, are difficult to interpret in black and white. The full colour images can be found in the on-line version, at doi:10.1016/j.actbio.2009.12.047.

References

[1] Shortkroff S, Spector M. Isolation and in vitro proliferation of chondrocytes, tenocytes, and ligament cells. In: Morgan JR, Yarmush ML, editors. Tissue engineering methods and protocols. Totowa, NJ: Humana Press; 1999. p. 195–203.
[2] Beskin JL, Sanders RA, Hunter SC, Hughston JC. Surgical repair of Achilles tendon ruptures. Am J Sports Med 1987;15:1–8.
[3] Chou L, Firth JD, Uitto VJ, Brunette DM. Substratum surface topography alters cell shape and regulates fibronectin mRNA level, mRNA stability, secretion and assembly in human fibroblasts. J Cell Sci 1995;108:1563–73.
[4] Choi CH, Hagvall SH, Wu BM, Dunn JC, Beygui RE, Kim CJ. Cell interaction with three-dimensional sharp-tip nanotopography. Biomaterials 2007;28:1672–9.
[5] Park A, Cima LG. In vitro cell response to differences in poly-L-lactide crystallinity. J Biomed Mater Res 1996;31:117–30.
[6] Baugh L, Vogel V. Structural changes of fibronectin adsorbed to model surfaces probed by fluorescence resonance energy transfer. J Biomed Mater Res A 2004;69:525–34.
[7] Baharloo B, Textor M, Brunette DM. Substratum roughness alters the growth, area, and focal adhesions of epithelial cells, and their proximity to titanium surfaces. J Biomed Mater Res A 2005;74:12–22.
[8] Keselowsky BG, Collard DM, Garcia AJ. Surface chemistry modulates fibronectin conformation and directs integrin binding and specificity to control cell adhesion. J Biomed Mater Res A 2003;66:247–59.
[9] Dunn G, Brown A. Alignment of fibroblasts on grooved surfaces described by a simple geometric transformation. J Cell Sci 1986;83:313–40.
[10] Wojciak-Stothard B, Curtis AS, Monaghan W, McGrath M, Sommer I, Wilkinson CD. Role of the cytoskeleton in the reaction of fibroblasts to multiple grooved substrata. Cell Motil Cytoskeleton 1995;31:147–58.
[11] Dalby MJ, Riehle MO, Sutherland DS, Agheli H, Curtis ASG. Use of nanotopography to study mechanotransduction in fibroblasts – methods and perspectives. Eur J Cell Biol 2004;83:159–69.
[12] Clark P, Connolly P, Curtis AS, Dow JA, Wilkinson CD. Topographical control of cell behaviour: II. Multiple grooved substrata. Development 1990;108:635–44.
[13] Britland S, Morgan H, Wojiak-Stodart B, Riehle M, Curtis A, Wilkinson C. Synergistic and hierarchical adhesive and topographic guidance of BHK cells. Exp Cell Res 1996;228:313–25.
[14] Kyoo Lee J, Baac H, Song SH, Lee SD, Park D, June Kim S. The topographical guidance of neurons cultured on holographic photo-responsive polymer. Conf Proc IEEE Eng Med Biol Soc 2004;7:4970–3.
[15] Hsu SH, Chen CY, Lu PS, Lai CS, Chen CJ. Oriented Schwann cell growth on microgrooved surfaces. Biotechnol Bioeng 2005;92:579–88.
[16] Miller C, Jeftinija S, Mallapragada S. Micropatterned Schwann cell-seeded biodegradable polymer substrates significantly enhance neurite alignment and outgrowth. Tissue Eng 2001;7:705–15.

[17] Thompson DM, Buettner HM. Schwann cell response to micropatterned laminin surfaces. Tissue Eng 2001;7:247–65.
[18] Wojciak-Stothard B, Madeja Z, Korohoda W, Curtis A, Wilkinson C. Activation of macrophage-like cells by multiple grooved substrata. Topographical control of cell behaviour. Cell Biol Int 1995;19:485–90.
[19] Andersson A, Bäckhed F, von Euler A, Richter-Dahlfors A, Sutherland D, Kasemo B. Nanoscale features influence epithelial cell morphology and cytokine production. Biomaterials 2003;24:3427–36.
[20] Dalby MJ, Riehle MO, Johnstone H, Affrossman S, Curtis AS. In vitro reaction of endothelial cells to polymer demixed nanotopography. Biomaterials 2002;23:2945–54.
[21] Thakar RG, Ho F, Huang NF, Liepmann D, Li S. Regulation of vascular smooth muscle cells by micropatterning. Biochem Biophys Res Commun 2003;307:883–90.
[22] Biela SA, Su Y, Spatz JP, Kemkemer R. Different sensitivity of human endothelial cells, smooth muscle cells and fibroblasts to topography in the nano–micro range. Acta Biomater 2009;5:2460–6.
[23] Curtis AS, Wilkinson CD, Crossan J, Broadley C, Darmani H, Johal KK, Jorgensen H, et al. An in vivo microfabricated scaffold for tendon repair. Eur Cell Mater 2005;9:50–7.
[24] Bosworth L, Clegg P, Downes S. Electrospun nanofibres of polycaprolactone, and their use for tendon regeneration. Int J Nano Biomaterials 2008;1:263–79.
[25] Cao Y, Vacanti JP, Ma X, Paige KT, Upton J, Chowanski Z, Schloo B, et al. Generation of neo-tendon using synthetic polymers seeded with tenocytes. Transplant Proc 1994;26:3390–2.
[26] Cao D, Liu W, Wei X, Xu F, Cui L, Cao Y. In vitro tendon engineering with avian tenocytes and polyglycolic acids: a preliminary report. Tissue Eng 2006;12:1369–77.
[27] Wang B, Liu W, Zhang Y, Jiang Y, Zhang WJ, Zhou G, Cui L, et al. Engineering of extensor tendon complex by an ex vivo approach. Biomaterials 2008;29:2954–61.
[28] Egerbacher M, Arnoczky SP, Caballero O, Lavagnino M, Gardner KL. Loss of homeostatic tension induces apoptosis in tendon cells: an in vitro study. Clin Orthop Relat Res 2008;466:1562–8.
[29] Lavagnino M, Arnoczky SP. In vitro alterations in cytoskeletal tensional homeostasis control gene expression in tendon cells. J Orthop Res 2005;23:1211–8.
[30] Aspenberg P. Reduced expression of BMP-3 due to mechanical loading: a link between mechanical stimuli and tissue differentiation. Acta Orthop Scand 2000;71:558–62.
[31] Arnoczky SP, Tian T, Lavagnino M, Gardner K. Ex vivo static tensile loading inhibits MMP-1 expression in rat tail tendon cells through a cytoskeletally based mechanotransduction mechanism. J Orthop Res 2004;22:328–33.
[32] Wojciak B, Crossan J, Curtis ASG, Wilkinson CDW. Grooved substrata facilitate in-vitro healing of completely divided flexor tendons. J Mater Sci Mater Med 1995;6:266–71.
[33] Keller S, Blagoi G, Lillemose M, Haefliger D, Boisen A. Processing of thin SU-8 films. J Micromech Microeng 2008;18:125020 (10pp).
[34] Waldron JWF, Wallace KD. Objective fitting of ellipses in the centre-to-centre (Fry) method of strain analysis. J Struct Geol 2007;29:1430–44.
[35] Stewart MC, Saunders KM, Burton-Wurster N, Macleod JN. Phenotypic stability of articular chondrocytes in vitro: the effects of culture models, bone morphogenetic protein 2, and serum supplementation. J Bone Miner Res 2000;15:166–74.
[36] Stewart MC, Kadlcek RM, Robbins PD, MacLeod JN, Ballock RT. Expression and activity of the CDK inhibitor p57Kip2 in chondrocytes undergoing hypertrophic differentiation. J Bone Miner Res 2004;19:123–32.
[37] Park J, Berthiaume F, Toner M, Yarmush ML, Tilles AW. Microfabricated grooved substrates as platforms for bioartificial liver reactors. Biotechnol Bioeng 2005;90:632–44.
[38] Arnoczky SP, Lavagnino M, Whallon JH, Hoonjan A. In situ cell nucleus deformation in tendons under tensile load; a morphological analysis using confocal laser microscopy. J Orthop Res 2002;20:29–35.
[39] Brunette DM, Kenner GS, Gould TR. Grooved titanium surfaces orient growth and migration of cells from human gingival explants. J Dent Res 1983;62:1045–8.
[40] Brunette DM. Spreading and orientation of epithelial cells on grooved substrata. Exp Cell Res 1986;167:203–17.
[41] Miller C, Shanks H, Witt A, Rutkowski G, Mallapragada S. Oriented Schwann cell growth on micropatterned biodegradable polymer substrates. Biomaterials 2001;22:1263–9.
[42] Recknor JB, Recknor JC, Sakaguchi DS, Mallapragada SK. Oriented astroglial cell growth on micropatterned polystyrene substrates. Biomaterials 2004;25:2753–67.
[43] Charest JL, Garcia AJ, King WP. Myoblast alignment and differentiation on cell culture substrates with microscale topography and model chemistries. Biomaterials 2007;28:2202–10.
[44] Liu Y, Ramanath HS, Wang DA. Tendon tissue engineering using scaffold enhancing strategies. Trends Biotechnol 2008;26:201–9.
[45] Hsu SH, Lu PS, Ni HC, Su CH. Fabrication and evaluation of microgrooved polymers as peripheral nerve conduits. Biomed Microdevices 2007;9:665–74.
[46] Baac H, Lee JH, Seo JM, Park TH, Chung H, Lee SD, Kim SJ. Submicron-scale topographical control of cell growth using holographic surface relief grating. Mater Sci Eng C: Biomimetic Supramol Syst 2004;24:209–12.
[47] Martinez E, Engel E, Planell JA, Samitier J. Effects of artificial micro- and nano-structured surfaces on cell behaviour. Ann Anat 2009;191:126–35.
[48] Papenburg BJ, Vogelaar L, Bolhuis-Versteeg LA, Lammertink RG, Stamatialis D, Wessling M. One-step fabrication of porous micropatterned scaffolds to control cell behavior. Biomaterials 2007;28:1998–2009.
[49] Patterson-Kane JC, Parry DA, Birch HL, Goodship AE, Firth EC. An age-related study of morphology and cross-link composition of collagen fibrils in the digital flexor tendons of young thoroughbred horses. Connect Tissue Res 1997;36:253–60.
[50] Lavagnino M, Arnoczky SP, Egerbacher M, Gardner KL, Burns ME. Isolated fibrillar damage in tendons stimulates local collagenase mRNA expression and protein synthesis. J Biomech 2006;39:2355–62.
[51] Wang JH, Jia F, Gilbert TW, Woo SL. Cell orientation determines the alignment of cell-produced collagenous matrix. J Biomech 2003;36:97–102.
[52] Wang JH, Grood ES, Florer J, Wenstrup R. Alignment and proliferation of MC3T3-E1 osteoblasts in microgrooved silicone substrata subjected to cyclic stretching. J Biomech 2000;33:729–35.
[53] Halasz K, Kassner A, Morgelin M, Heinegard D. COMP acts as a catalyst in collagen fibrillogenesis. J Biol Chem 2007;282:31166–73.
[54] Goodman SA, May SA, Heinegard D, Smith RK. Tenocyte response to cyclical strain and transforming growth factor beta is dependent upon age and site of origin. Biorheology 2004;41:613–28.
[55] Pietak A, McGregor A, Gauthier S, Oleschuk R, Waldman SD. Are micropatterned substrates for directed cell organization an effective method to create ordered 3D tissue constructs? J Tissue Eng Regen Med 2008;2:450–3.
[56] Lin YL, Jen JC, Hsu SH, Chiu IM. Sciatic nerve repair by microgrooved nerve conduits made of chitosan–gold nanocomposites. Surg Neurol 2008;70(Suppl. 1):9–18.
[57] Hsu SH, Ni HC. Fabrication of the microgrooved/microporous polylactide substrates as peripheral nerve conduits and in vivo evaluation. Tissue Eng A 2009;15:1381–90.